

DETC2011-4+&, -

MULTIPLE LIMIT CYCLES IN LASER INTERFERENCE TRANSDUCED RESONATORS

David B. Blocher *

Theoretical and Applied Mechanics
Cornell University
Ithaca, New York 14850
Email: dbb74@cornell.edu

Richard H. Rand

Department of Mechanical
and Aerospace Engineering
Cornell University
Ithaca, New York 14850

Alan T. Zehnder

Department of Mechanical
and Aerospace Engineering
Cornell University
Ithaca, New York 14850

ABSTRACT

Nanoscale resonators whose motion is measured through laser interferometry are known to exhibit stable limit cycle motion. Motion of the resonator through the interference field modulates the amount of light absorbed by the resonator and hence the temperature field within it. The resulting coupling of motion and thermal stresses can lead to self oscillation, i.e. a limit cycle. In this work the coexistence of multiple stable limit cycles is demonstrated in an analytic model. Numerical continuation and direct numerical integration are used to study the structure of the solutions to the model. The effect of damping is discussed as well as the properties that would be necessary for physical devices to exhibit this behavior.

INTRODUCTION

Due to their high frequencies and ease of integration with traditional electronics, MEMS resonators have found a variety of uses in the past decade from electrical filters [1] to mass detection sensors [2] and reference oscillators [3]. Many of these applications make use of the oscillator's sharply peaked resonance curve. In these applications, self-resonant systems or limit cycle oscillators have the added benefit of not requiring a separate on-chip modulated drive to achieve periodic motion. Langdon and Dowe [4] first demonstrated optically driven self oscillation in a MEMS device. They showed that an optically thin MEMS de-

vice suspended over a reflective substrate sets up a Fabry-Pérot interferometer which couples absorption of light to displacement of the device. Thus, illuminating MEMS beams with an continuous wave (CW) unmodulated laser causes optical-thermal-mechanical feedback. When the laser intensity is low, the beam bends statically, but for high enough laser power the beam begins to self-oscillate. Later work examined the necessary conditions for self oscillation [5–7]. See [8] for an overview of limit cycles in optically driven MEMS.

Our research analyzes the mechanisms of self oscillation in these devices, and focuses on the resultant dynamics. Previous work [8, 9] on modeling the dynamics of limit cycle oscillations in optically driven MEMS resonators has assumed small displacement and expanded the function describing the interference field in a power series, losing the periodicity in the process. In this work, we treat the case where displacement is not small and show that a periodic interference field suggests the coexistence of multiple stable limit cycles. To our knowledge, multiple *stable* limit cycles have not been predicted or seen experimentally in previous work on MEMS. Devices exhibiting multiple stable limit cycles would allow for tuning between distinct frequency bands, and within them in applications such as GPS receivers. On the other hand, extraneous stable motions could be problematic if a device designed to operate in one limit cycle was found to operate in a different limit cycle with a different frequency and amplitude.

In the following section, the resonators are described, the

*Address all correspondence to this author.

equations of motion used to model them derived, and model parameters identified. In subsequent sections continuation and direct integration results are presented and discussed. Since we do not assume small displacement, approximate analytic methods (Lindstedt's method, harmonic balance) give poor predictions, thus no analytic results are presented. Lastly conclusions are drawn about the properties of the corresponding physical devices in which multiple stable limit cycles would be possible.

INTERFEROMETRIC TRANSDUCTION

In self-resonant MEMS, laser interference transduction drives the resonator and provides a way to measure the motion. A typical experimental setup is shown in Figure 1. Devices are fabricated from a thin film stack to create an optically thin resonator suspended over a thick substrate. A CW laser is focused on the resonator, mounted in vacuum to reduce viscous damping. The resonator-gap-substrate system sets up a Fabry-Pérot interferometer whose absorbed signal depends on the device gap. As the resonator moves through interference field, it modulates the reflected signal which is measured in an AC-coupled photodiode. This general setup has been used to excite and study oscillations in cantilevers, clamped-clamped beams, disks, and domes [8, 10, 11].

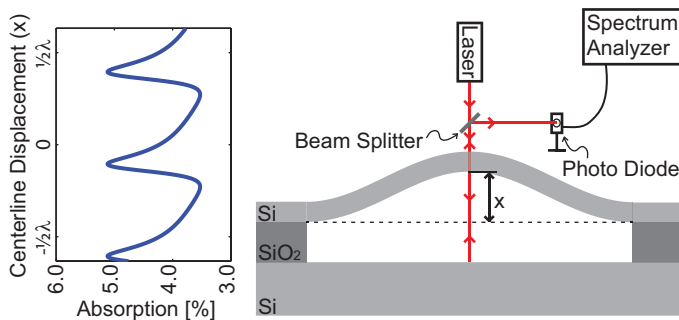


FIGURE 1. CROSS-SECTIONAL VIEW OF AN INTERFEROMETRICALLY TRANSDUCED CLAMPED-CLAMPED MEMS BEAM. INSET IS A PLOT OF THE LASER ENERGY ABSORBED AS A FUNCTION OF THE CENTERLINE DISPLACEMENT (x) MEASURED WITH RESPECT TO THE UNDEFLECTED CONFIGURATION. AS THE BEAM DEFLECTS, IT CHANGES THE GAP TO SUBSTRATE AND MODULATES THE ABSORPTION. THUS THE INTERFEROMETER COUPLES HEATING TO DISPLACEMENT. THE ABSORPTION IS PERIODIC IN $\frac{\lambda}{2}$.

THEORETICAL MODEL

The equations that follow are applicable to any interferometrically-driven MEMS device with a temperature dependent stiffness and direct thermal-mechanical coupling, but here a clamped-clamped beam is modeled to illustrate the phenomenon. A similar model has been used to describe the motion of optically excited disks, dome oscillators, and beams [8, 10, 12, 13]. See [10] for a more detailed discussion. Although the devices have spatially varying fields, first-mode vibration is assumed, and the centerline displacement (x) as depicted in Figure 1 is modeled as a one degree-of-freedom oscillator. A quasi-static temperature field is assumed, and the average temperature in the device (T) modeled using a lumped thermal model. No external forcing is applied to the system.

Though membrane stress is neglected in linear beam theory, it is an important non-linearity for high curvature deformations in structures. For pre-buckled beams subject to out of plane loads, the slope of a force vs. displacement curve increases with displacement due to membrane stresses, a phenomenon called "hardening." Membrane stress has been shown to come into an oscillator model of first mode vibration as a cubic stiffness ($\tilde{\beta}x^3$) which is hardening ($\tilde{\beta} > 0$) for pre-buckled beams [14] and softening ($\tilde{\beta} < 0$) for post-buckled beams [15]. As a result, a cubic stiffness term is included to incorporate the affect of membrane stiffness.

The temperature above ambient in the beam (T) leads to an increase in compressive stress at the support needed to counteract thermal strain. It is known that the first mode frequency of a clamped-clamped beam decreases monotonically as the compression is increased until it reaches zero frequency at the buckling load [16]. Thus the stiffness of the beam to out of plane displacements is a decreasing function of temperature. In order to account for the dependence of frequency on temperature the linear spring stiffness is modeled as a decreasing function of temperature: $k = k_0(1 - \tilde{c}_1 T)$, where the spring stiffness temperature coefficient (\tilde{c}_1) determines how strongly the frequency depends on temperature. This recovers the theoretical resonant frequency exactly for pre-buckled beams [16] and approximately for post-buckled beams [17].

Finally, it has been observed that heating of cantilever beams causes static deflection due to stress gradients at the anchor points [18]. FEM modeling indicates that the same is true for clamped-clamped beams [19]. To incorporate this direct change in displacement due to temperature a term proportional to the temperature ($\tilde{c}_2 T$) is included in the mechanical model which shifts the equilibrium solution as the temperature increases. The thermo-mechanical coupling coefficient (\tilde{c}_2) is the deflection for a unit temperature change. Including a damping term, along with the terms previously described, and non-dimensionalizing, gives the following mechanical model

$$\ddot{z} + \frac{\dot{z}}{Q} + (1 - c_1 T)z + \beta z^3 = c_2 T, \quad (1)$$

where z is the centerline displacement scaled by the laser wavelength ($z = \frac{x}{\lambda}$), time is rescaled by the linear resonant frequency ($\tau = t\omega_0$), overdots denote derivatives with respect to non-dimensional time τ , and the parameters $\tilde{\beta}, \tilde{c}_1, \tilde{c}_2$ have been transformed to the dimensionally appropriate β, c_1, c_2 .

The resonator is assumed to heat up due to laser absorption and cool down due to Newton's law of cooling, giving the following equation governing the average temperature in the beam (T)

$$\dot{T} = -BT + HP_{absorbed}(z), \quad (2)$$

where B is the cooling rate due to conduction, H is the inverse of the lumped thermal mass, and $P_{absorbed}(z)$ is the energy absorbed due to interferometric heating. Once again, overdots represent derivatives with respect to non-dimensional time τ . Note that the function $P_{absorbed}(z)$ depends on the properties of the interferometer for a given deflection (z) and is proportional to the applied laser power. $P_{absorbed}(z)$ can be described numerically using an optical model presented in [20]. The resulting function is periodic with period $\frac{\lambda}{2}$ in x (or $\frac{1}{2}$ in z) and is approximated by

$$P_{absorbed}(z) = P[\alpha + \gamma \sin^2(2\pi(z - z_o))] \quad (3)$$

with fitting parameters α, γ , and z_o . Equations (1, 2, 3) form a system of 2 coupled ordinary differential equations and one algebraic equation to model the first mode of vibration of a MEMS resonator. In the next section, the parameter estimation process is described and parameters are established for a 201nm thick, 10 μ m long clamped-clamped silicon beam with 400nm gap to substrate, subjected to 50MPa of pre-compression.

PARAMETER ESTIMATION

Estimation of the physical, thermal, and optical parameters are done using a number of different analyzes. The optical parameters α, γ , and z_o are least squares fit to the numerical results from the model presented in [20]. Given the complex index of refraction of the materials as well as the resonator thickness and gap to substrate, the code given in [20] solves Maxwell's equations to determine the percentage of laser energy absorbed in and reflected from the resonator. The gap to substrate is varied to account for deflection of the device, giving a result seen in Figure

1. For the 201nm thick silicon device with 400nm un-deflected gap to substrate, we estimate $\alpha \simeq 0.035, \gamma \simeq 0.011, z_o \simeq 0.18$.

The mechanical parameters are fit as follows: first the devices under test are driven at low amplitude in vacuum and their resonance curve is measured. The quality factor (Q) is determined by fitting the resonance curve to a Lorentzian, and is estimated to be $Q = 13,800$. Given the low damping, the natural frequency (ω_0) is taken to be equal to the resonant frequency ($w_r = 9.96MHz$) which is used to non-dimensionalize the equations. The spring stiffness temperature coefficient ($c_1 = 0.00475K^{-1}$) is determined by taking a Taylor series expansion of the frequency-compression relation given in [16], using linear thermoelasticity to convert between temperature above ambient and compression. The cubic stiffness ($\beta = 4.65$) is estimated using an FEM analysis in which a normal load of 0 – 10 μ N is applied at the center of a clamped-clamped beam. The load-displacement curve is least squares fit to $F = kz + \beta z^3$ using the appropriate non-dimensionalization.

The thermal parameters are also fit using an FEM analysis. The beam and a large volume of the surrounding substrate are modeled in 3D. The temperature is assumed to be zero at the outer boundary and a Heaviside unit flux is applied at the center of the beam. The inverse lumped thermal mass (H) is related to the slope of the temperature at time $t = 0$ ($\dot{T}|_{t=0} = H$) and the cooling rate due to conduction (B) is related to the steady state average temperature ($\lim_{t \rightarrow \infty} T(t) = \frac{H}{B}$).

To determine c_2 , equivalent thermal stresses are calculated from the steady state temperature field and applied to the mechanical model. The normalized centerline deflection for unit temperature rise is the thermal coupling coefficient (c_2). See Table 1 for a full list of material properties and parameters estimated.

CONTINUATION RESULTS

The continuation tool AUTO 2000 [21, 22], is used to examine the structure of solutions to equations (1,2,3). This software package is commonly used in the bifurcation analysis of differential equations and algebraic systems. Using AUTO 2000 we track the change in the equilibrium and periodic solutions as the laser power is varied.

We begin with $P = 0$ which has known equilibrium solution ($z = 0, \dot{z} = 0, T = 0$). This equilibrium solution is continued in P , monitoring the eigenvalues of the Jacobian of the linearized system for Hopf-bifurcations. For low laser power, there is a unique stable equilibrium solution with small centerline displacement. As the laser power is increased to $P \simeq 18mW$, this equilibrium solution loses stability in a Hopf bifurcation leading to self-oscillation. As the power is increased further, the equilibrium solution branch begins to lift up from $z_{eq} = 0$ and a second branch of equilibrium solutions is born at $P \simeq 168mW$ in a fold

Material Properties	Si	(SiO ₂) [units]	Model Parameters
Density, ρ	2420	(2200) [$\frac{kg}{m^3}$]	Q 13,800
Poisson Ratio, ν	0.279	(0.17)	c_1 4.75×10^{-3} [K^{-1}]
Young's Modulus, E	130	(70) [GPa]	c_2 1.37×10^{-5} [K^{-1}]
CTE, α_T	2.5	(0.5) [$\frac{\mu m}{K}$]	β 4.65
Thermal Conductivity, k	170	(1.38) [$\frac{W}{m \cdot K}$]	H 4410 [$\frac{K}{W}$]
Specific Heat Capacity, c	712	(1120) [$\frac{J}{kg \cdot K}$]	B 0.152
Index of Refraction (\bar{n}):			γ 0.011
$Re(\bar{n})$	3.882	(N/A)	α 0.035
$Im(\bar{n})$	-0.019	(N/A)	z_0 0.18

TABLE 1. MATERIAL PROPERTIES USED IN PARAMETER ESTIMATION, AND ESTIMATED PARAMETERS USED IN SUBSEQUENT CONTINUATION AND INTEGRATION OF MODEL EQUATIONS, FOR 201nm THICK, 10 μ m LONG BEAMS.

of equilibrium points. An equilibrium point along this branch is computed numerically using a root finding method and then is used as a starting point for continuation of the branch. See Figure 2 for a plot of the equilibrium branches along with Hopf-bifurcation points at which limit cycles are born. This behavior in the position and number of equilibria is caused by asymmetric buckling in the model. Hopf bifurcations along the branches of equilibria alter the usual buckling stability result - that the unbuckled state is unstable and the buckled states stable.

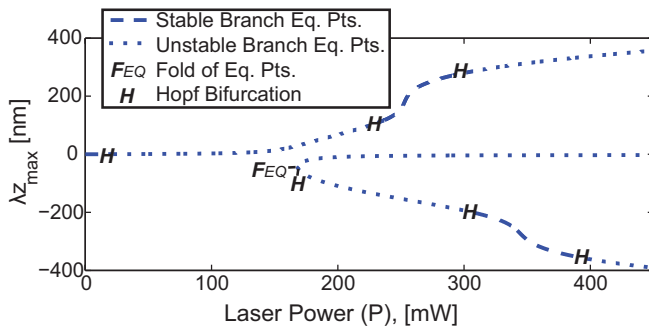


FIGURE 2. AUTO GENERATED BIFURCATION DIAGRAM OF THE SYSTEM, SHOWING LOCATION AND STABILITY OF EQUILIBRIUM SOLUTIONS AS A FUNCTION OF LASER POWER (P). LIMIT CYCLE BRANCHES EMERGING FROM HOPF BIFURCATIONS (H) ARE SHOWN IN FIGURE 9.

Next, we turn our attention to the limit cycle oscillations born in Hopf bifurcations. The continuation is restarted at each

Hopf bifurcation and the emerging limit cycle is followed, allowing the power P and frequency of oscillation ω to vary. Following the limit cycle branch born in the first Hopf bifurcation, we see a series of folds of limit cycles in which stable and unstable limit cycles coalesce or divide (see Figure 3), in addition to regions of period doubling which are discussed later. Note that for a given laser power, the amplitudes of stable limit cycles differ by roughly the period of the interferometer, $\frac{\lambda}{2} \sim 316nm$. Thus the multiplicity of stable limit cycles is due to periodicity in the interference field, and each higher amplitude stable limit cycle shows motion between similar points in the phase of the interference field, but includes more or less periods. For example, if the lowest amplitude limit cycle shows motion between one peak of absorption in the interference field and the first subsequent peak in the interference field, then the second lowest amplitude limit cycle shows motion between one peak of the absorption in the interference field, and the second subsequent peak (see Figure 1). See Figure 4 for a phase portrait of the equilibrium solution and limit cycles for $P = 135mW$ when a stable and unstable limit cycle have just been born in a fold of limit cycles.

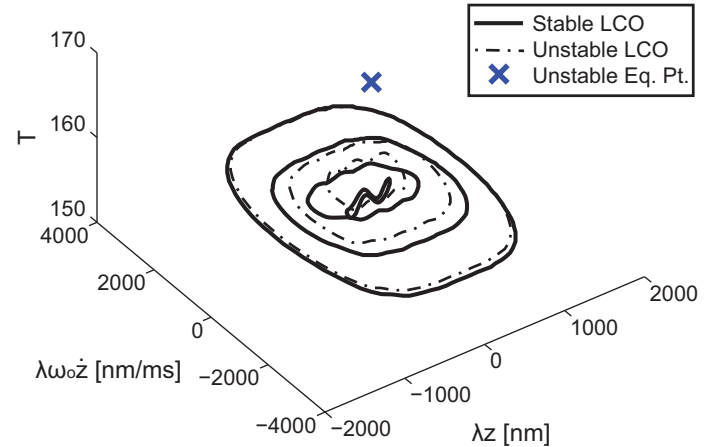


FIGURE 4. PLOT OF THE EQUILIBRIUM AND PERIODIC SOLUTIONS FOR $P = 135mW$. NOTE THAT LARGE AMPLITUDE STABLE AND UNSTABLE MOTIONS HAVE JUST BEEN BORN IN A FOLD OF LIMIT CYCLES. SEE FIGURE 3 FOR THE ACCOMPANYING BIFURCATION DIAGRAM.

The period of oscillation along the first Hopf branch is depicted in Figure 5. Note that the limit cycle initially has non-dimensional period of $\sim 2\pi$. As the laser power is increased two competing factors influence the period of oscillation. The temperature dependence of the linear stiffness causes the period to increase with temperature and so the period increases with laser power for a given stable limit cycle. At the same time, the cubic stiffness due to membrane stresses causes the period to decrease

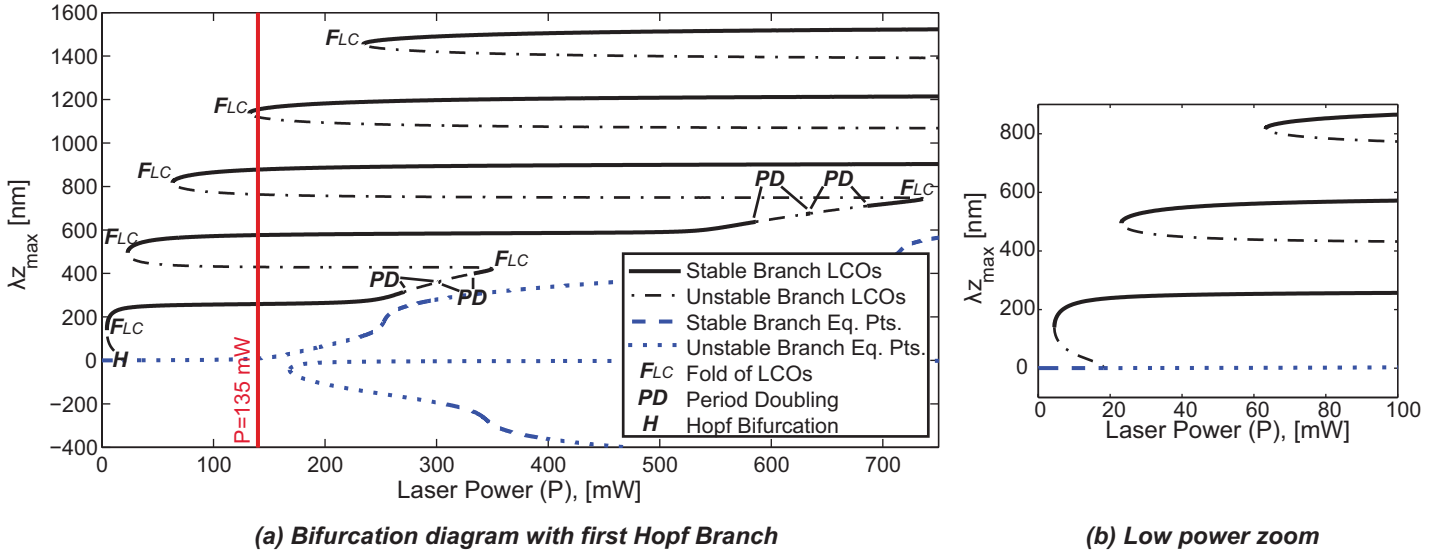


FIGURE 3. AUTO GENERATED BIFURCATION DIAGRAM (a) SHOWING THE TWO BRANCHES OF EQUILIBRIUM SOLUTIONS AS WELL AS THE BRANCH OF LIMIT CYCLES BORN IN THE FIRST HOPF BIFURCATION. INCLUDED IS A ZOOM VIEW (b) OF THE BIFURCATION DIAGRAM FOR LOW LASER POWER. IN ORDER TO DISPLAY THE EQUILIBRIUM SOLUTIONS AND PERIODIC MOTIONS ON THE SAME PLOT, WE USE THE MAXIMUM z -VALUE ATTAINED IN ONE CYCLE (z_{max}) AS THE DEPENDENT VARIABLE WHEN PLOTTING LIMIT CYCLES. THIS MEASURE INCLUDES THE AMPLITUDE OF OSCILLATION PLUS A SMALL MEAN VALUE ROUGHLY EQUAL TO THE z -VALUE OF THE EQUILIBRIUM SOLUTION FROM WHICH THE MOTION WAS BORN. THE INTERSECTION OF A VERTICAL LINE WITH EQUILIBRIUM OR LIMIT CYCLE BRANCHES INDICATES THE SOLUTIONS POSSIBLE AT A GIVEN LASER POWER. SEE FIGURE 4 FOR A PHASE PORTRAIT OF THE LIMIT CYCLES AND EQUILIBRIUM SOLUTIONS FOR $P = 135mW$.

with increasing amplitude of oscillation. Thus at a fixed laser power, high amplitude limit cycles have lower periods.

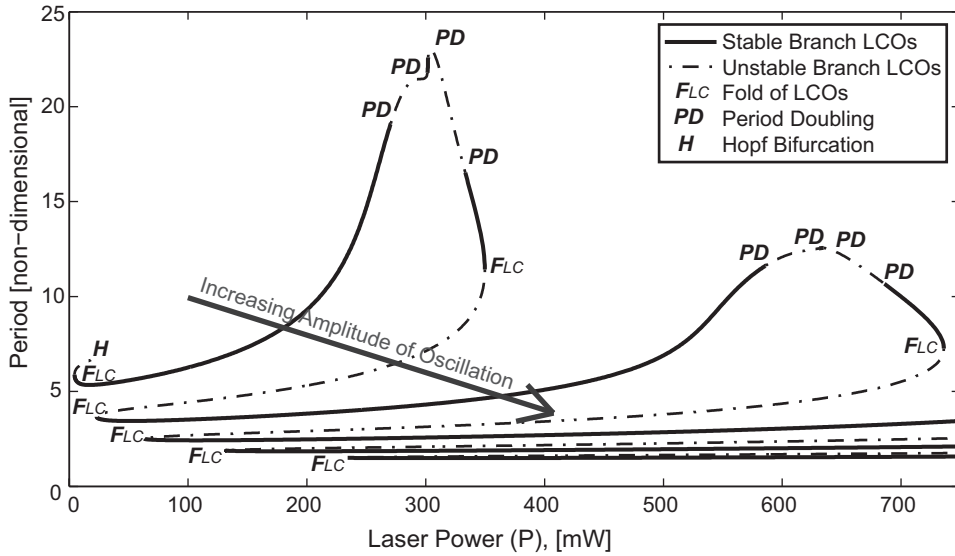
It is numerically observed that as damping is increased, high amplitude limit cycles become unattainable at low laser power. Thus increased damping flattens out these curves in the first Hopf branch, reducing the number of stable limit cycles accessible at a given laser power (see Figure 6). For sufficiently high damping, the Hopf bifurcation becomes supercritical and a unique stable limit cycle exists in this branch for $P > P_{Hopf}$.

Although the results presented here are for $10 \mu m$ beams subject to 50MPa of pre-compression, we have estimated parameters for beams of length 7,10,15 & 20 μm with varying amounts of pre-compression. Continuation of the model equations using these parameters shows that multiplicity of stable limit cycles in the first Hopf branch is a *robust feature of the model* for lightly damped pre-buckled beams, and occurs at laser powers which are realizable in experimental setups. In the following section, we describe the rest of the bifurcation structure for 10 μm beams, including bifurcations occurring at laser powers above the thermal buckling power. We also describe the jump phenomenon associated with destruction of stable limit cycles.

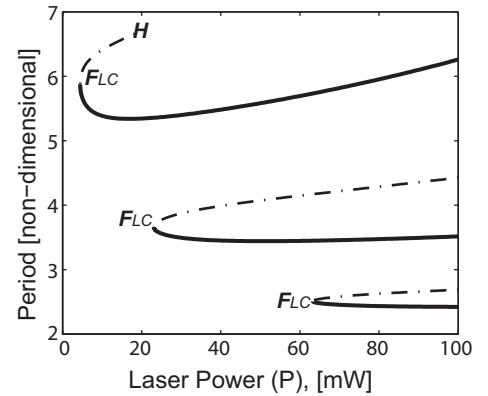
COMPLETE BIFURCATION DIAGRAM

In this section we build up the complete picture of the bifurcation structure, by describing each additional bifurcation separately. To begin with, we return to the regions of period doubling along the first Hopf branch (see Figure 3). Here we see that as we increase the laser power, our original limit cycle goes unstable and a new stable limit cycle is born with twice the period of the original. Continuing this new limit cycle, there is a cascade of period doubling where this process continues with increasing frequency as we increase the laser power (see Figure 7). Direct numerical integration is used to verify the existence of these special solutions.

For all of the parameter sets studied, there were additional Hopf bifurcations from the equilibrium branches for laser powers above the buckling power. Following the limit cycle emerging from the second Hopf bifurcation, we see a fold of limit cycles, and then the cycle coalesces with an unstable equilibrium point in a homoclinic bifurcation. See Figure 8 for a bifurcation diagram of this region and a phase portrait just before the homoclinic bifurcation. Accounting for the limit cycles born in the other Hopf bifurcations gives a complete bifurcation diagram shown in Figure 9.

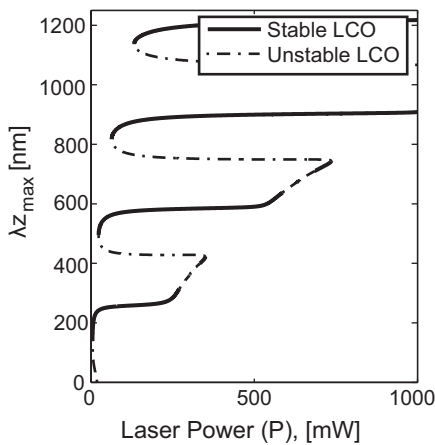


(a) Period of oscillation along the first Hopf branch

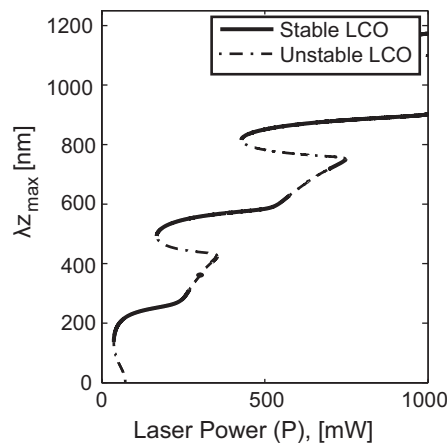


(b) Low power zoom

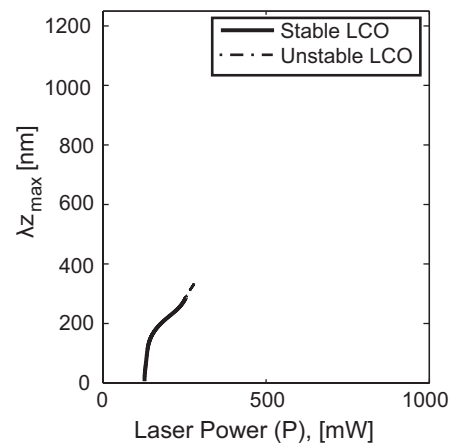
FIGURE 5. THE PERIOD OF OSCILLATION (a) ALONG THE BRANCH OF LIMIT CYCLES BORN IN THE FIRST HOPF. INCLUDED IS A ZOOM VIEW (b) OF THE PERIOD FOR LOW LASER POWER. NOTE THAT THE LIMIT CYCLE IS BORN WITH NON-DIMENSIONAL PERIOD $\sim 2\pi$ AT THE POINT MARKED *H*.



(a) $Q=14,000$

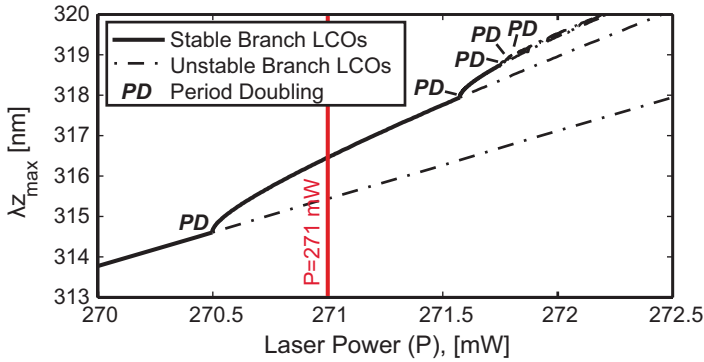


(b) $Q=1,400$

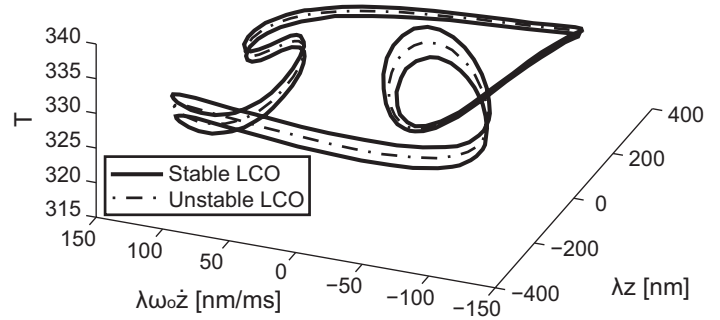


(c) $Q=140$

FIGURE 6. EFFECT OF DAMPING: AUTO GENERATED BIFURCATION DIAGRAM SHOWING THE BRANCH OF LIMIT CYCLES BORN IN THE FIRST HOPF BIFURCATION. THE SAME MODEL PARAMETERS ARE USED AS BEFORE, EXCEPT THE QUALITY FACTOR (Q) IS REDUCED BY A FACTOR OF 10 BETWEEN EACH SUBPLOT. NOTE THAT INCREASED DAMPING INCREASES THE LASER POWER AT WHICH SELF OSCILLATION BECOMES POSSIBLE, AND ALSO FLATTENS OUT THE CURVES IN THE FIRST HOPF BRANCH. FOR $Q = 140$, THE HOPF BIFURCATION HAS BECOME SUPERCRITICAL AND THERE IS A UNIQUE STABLE LIMIT CYCLE, WHICH QUICKLY LEADS TO PERIOD DOUBLING AND DIES IN A HOMOCLINIC BIFURCATION (*NOT SHOWN*).



(a) Bifurcation diagram with region of period doubling



(b) Phase portrait for P=271 mW

FIGURE 7. BIFURCATION DIAGRAM (a) OF A CASCADE OF PERIOD DOUBLING FOR HIGH LASER POWER. ONLY THE FIRST FIVE PERIOD DOUBLING BIFURCATIONS ARE TRACKED NUMERICALLY, THOUGH MORE ARE BELIEVED TO EXIST. PERIOD DOUBLING IS A WELL-KNOWN ROUTE TO CHAOS, AND IT IS LIKELY THAT CHAOS EXISTS IN THE MODEL IN THIS RANGE OF LASER POWERS. A PHASE PORTRAIT (b) JUST AFTER THE FIRST PERIOD DOUBLING BIFURCATION SHOWS THAT THE ORIGINAL LIMIT CYCLE (ONE-LOOP) HAS GONE UNSTABLE, AND A NEW STABLE CYCLE IS BORN WHICH TRAVERSES TWO LOOPS BEFORE CLOSING.

JUMP PHENOMENON

Finally, we use direct integration to illustrate the hysteresis possible in the system. Although the bifurcation structure illustrates the types of stable and unstable behaviors possible in the model as we increase or decrease the laser power, it does not tell us which behaviors would be seen experimentally as we change the laser power - a question dealing with the basins of attraction for different stable behaviors. For each Hopf bifurcation or fold of limit cycles where an equilibrium solution loses stability or stable motion disappears, respectively, we use a point along that motion as an initial condition, increase or decrease the laser power slightly beyond the bifurcation and integrate until the trajectory settles onto a new steady behavior. See Figure 10 for a plot of the jump phenomenon. As we quasi-statically increase the laser power from zero beyond the first Hopf bifurcation at $P \sim 18mW$, the beam begins to oscillate in the lowest amplitude limit cycle. Once oscillating, we have to decrease the power below the lowest fold of limit cycles at $P \sim 4.5mW$ in order to jump back onto the stable equilibrium solution. At each fold of limit cycles along the first Hopf branch, jumps occur up to the next highest amplitude stable limit cycle when increasing the laser power, or down to the next lowest amplitude stable limit cycle when decreasing the laser power. Entering the region of period doubling, stable n -cycles give rise to stable $2n$ -cycles and so there are no jumps. However, it is unclear if stable periodic motions exist over the entire interval or if there are regions of chaos.

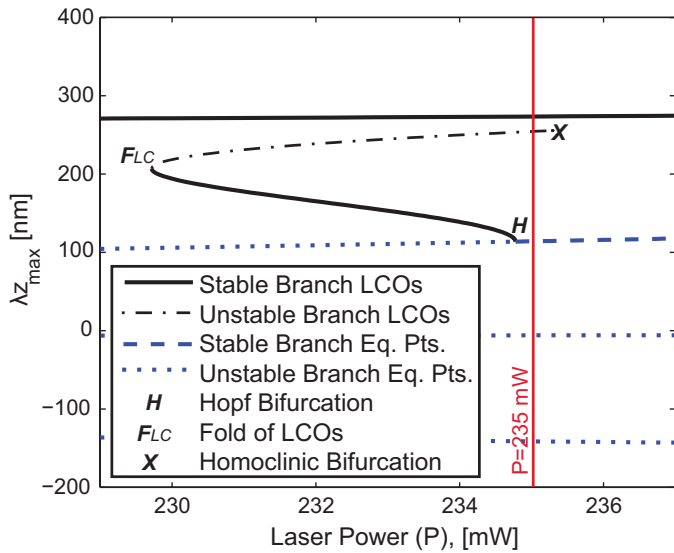
COMPARISON WITH PREVIOUS WORK

Previous work [8, 9] on modeling limit cycle oscillations in optically driven MEMS resonators has assumed small displacement, and expanded the optical equation (3) in a power series losing the periodicity in the process, but making the equations amenable to approximate analytic methods. This small displacement approximation predicts a single Hopf bifurcation, either subcritical or supercritical, leading to a stable/unstable pair or single stable limit cycle respectively. Thus series expanding the optical equation suppresses secondary Hopf bifurcations and folds of limit cycles. For comparison, a bifurcation diagram for equations (1,2) is given in Figure (11), where the parameters from Table 1 are used but equation (3) has been Taylor expanded in z , keeping the first 2 terms.

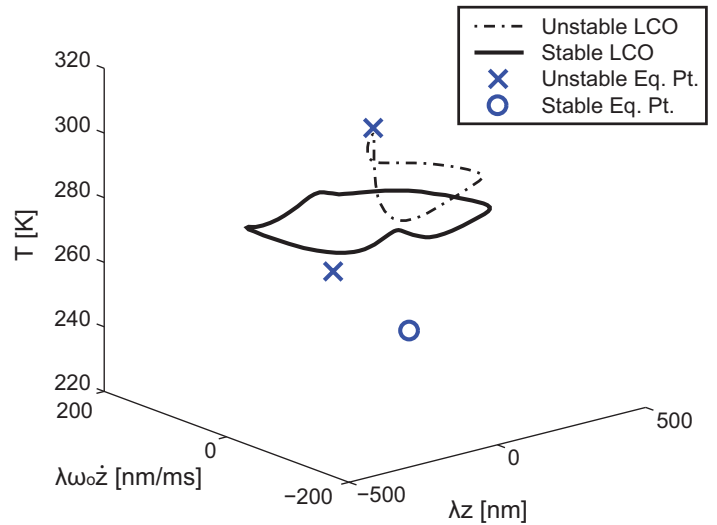
CONCLUSION

A MEMS device illuminated within an interference field will self-oscillate due to feedback between absorption and displacement. Models in the form of coupled differential equations have been used to describe the dynamics of such vibrations [6, 8–10, 12, 13, 23, 24], and analyzed under the assumption of small displacement. In this work, we show that if we relax that assumption then multiple stable limit cycles are possible due to the periodicity of the interference field. The frequency of these oscillation is shown to depend sensitively on the laser power, and other complex motions exist for high laser power.

The analysis presented is applicable to any interferometrically driven MEMS device with a temperature dependent stiffness and static deflection, though clamped-clamped beams were chosen to analyze here due to their relatively simple structure.



(a) Bifurcation diagram with second Hopf branch



(b) Phase portrait for P=235 mW

FIGURE 8. PORTION OF BIFURCATION DIAGRAM (a) IN THE REGION OF THE SECOND HOPF POINT (AFTER THE THERMAL BUCKLING POINT AS SEEN IN FIGURE 9), AND PHASE PORTRAIT (b) OF THE SYSTEM JUST BEFORE THE HOMOCLINIC BIFURCATION. NOTE IN THE PHASE PORTRAIT THAT THE UNSTABLE LIMIT CYCLE HAS DEVELOPED A KINK AS IT APPROACHES THE STABLE AND UNSTABLE MANIFOLD OF AN EQUILIBRIUM POINT. INCLUDED IS THE NEIGHBORING LIMIT CYCLE FROM THE FIRST HOPF BRANCH. OTHER HIGHER AMPLITUDE LIMIT CYCLES FROM THE FIRST HOPF BRANCH WHICH DO NOT SHOW IN THIS REGION OF THE BIFURCATION DIAGRAM ARE OMITTED FROM THE PHASE PORTRAIT, THOUGH THESE MOTIONS EXIST FOR THIS LASER POWER.

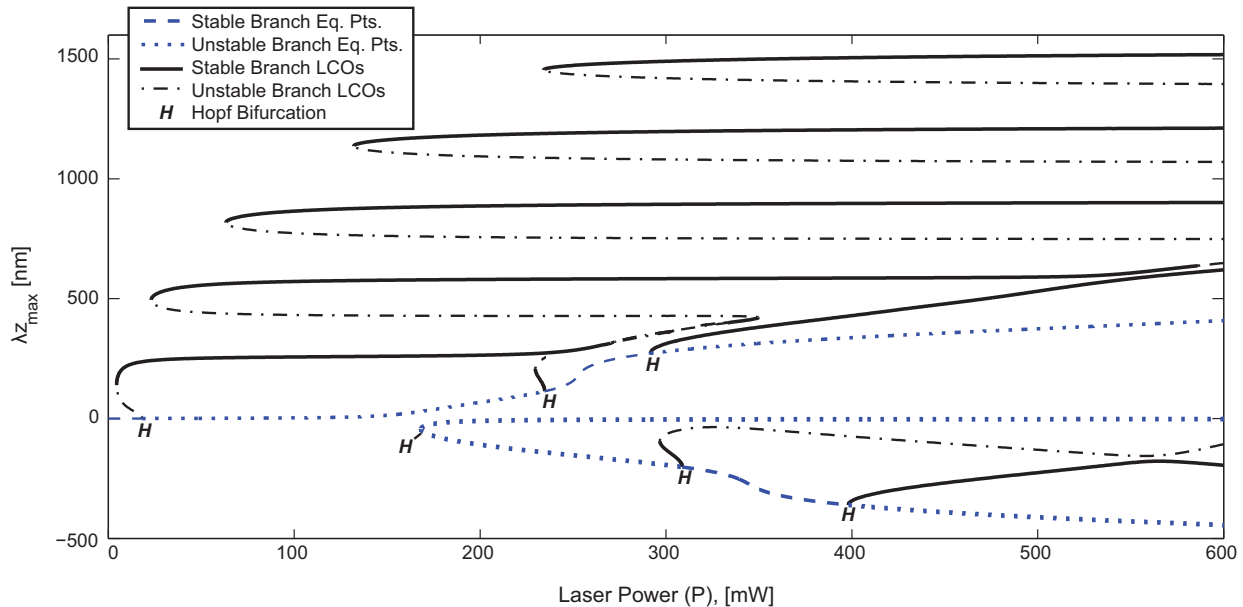


FIGURE 9. COMPLETE BIFURCATION DIAGRAM OF THE SYSTEM. NOTE THAT THE LIMIT CYCLE OSCILLATION BORN IN A HOPF BIFURCATION IN THE ELBOW OF THE FOLD OF EQUILIBRIA DIES SO QUICKLY IN A HOMOCLINIC BIFURCATION THAT IT IS NOT VISIBLE ON THE BIFURCATION DIAGRAM AT THIS SCALE.

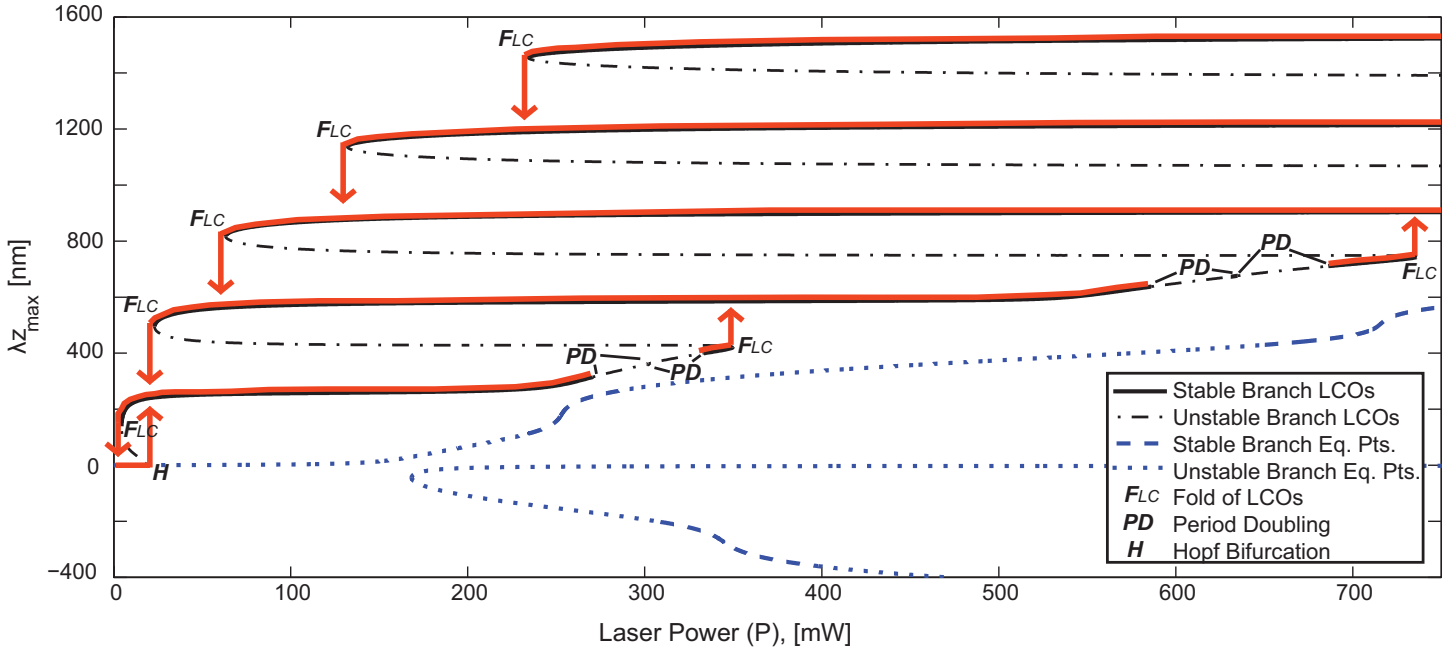


FIGURE 10. JUMP PHENOMENON IN THE FIRST HOPF BRANCH.

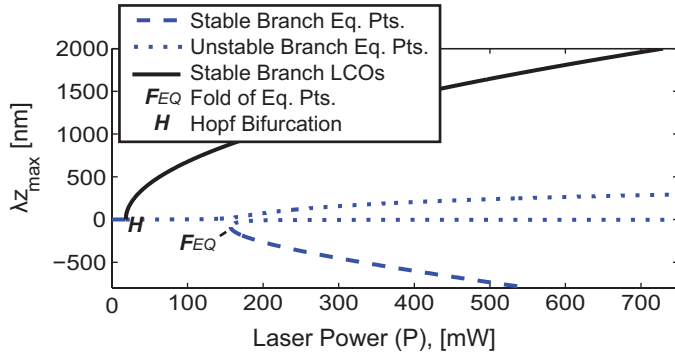


FIGURE 11. BIFURCATION DIAGRAM OF THE MODEL EQUATIONS ASSUMING SMALL DISPLACEMENT, WHERE EQUATION (3) HAS BEEN EXPANDED IN A FIRST ORDER TAYLOR SERIES. BUCKLING HAS NOT BEEN SUPPRESSED, BUT SECONDARY HOPF BIFURCATIONS AND FOLDS OF LIMIT CYCLES HAVE BEEN LOST. THE APPROXIMATE EQUATIONS GIVE THE CORRECT VALUE FOR P_{HOPF} BUT NOT OF THE LIMIT CYCLE AMPLITUDE OR EQUILIBRIUM SOLUTION.

Physical devices exhibiting multiple stable limit cycles due to the phenomenon presented are expected to share some common characteristics:

- (a) The need for a temperature dependent stiffness and deflection suggests the use of devices that can generate tension across the device, i.e. clamped-clamped beams or domes

rather than cantilevers or disks.

- (b) Damping has been shown to decrease the number of stable limit cycles accessible at a given power, thus devices would need to be high-Q.
- (c) Stable limit cycles are seen to be separated in amplitude by $\Delta x \simeq \frac{\lambda}{2}$. To permit n -stable limit cycles, devices must have a initial gap-to-substrate of greater than $\frac{\lambda}{2}$ in order to prevent contact with the substrate. Excitation with a HeNe laser would require a gap of $\gtrsim 1\mu m$ in order to see three limit cycles.

Although rigorously derived and analyzed, the results are expected only to present a qualitative picture of the dynamics of interferometrically driven MEMS devices, i.e. that multiple stable periodic motions are to be expected in large clamped-clamped beams and domes in low damping environments. Note that these motions are seen for low laser powers (below the buckling temperature). Above the buckling temperature, the frequency-compression relationship changes, and the model may lose validity. A description of the bifurcation structure in this region of high laser power ($P > 168mW$ for the parameters used here) is presented and represents simply an analysis of the model, which suggests the possibility of period doubling, chaos, and secondary Hopf bifurcations in the physical system.

ACKNOWLEDGMENT

This work is supported under NSF grant #0600174 and was performed in part at the Cornell NanoScale Facility, a member

of the National Nanotechnology Infrastructure Network, which is supported by the National Science Foundation (Grant ECS-0335765). This work also made use of the Cornell Center for Materials Research Facilities supported by the National Science Foundation under Award Number DMR-0520404.

REFERENCES

- [1] Lin, L., Howe, R. T., and Pisano, A. P., 1998. "Microelectromechanical filters for signal processing". *J. Microelectromech. Syst.*, **7**(3), pp. 286–294.
- [2] Ilic, B. R., Czaplewski, D. A., Craighead, H. G., Neuzil, P., Campagnolo, C., and Batt, C. A., 2000. "Mechanical resonant immunospecific biological detector". *Appl. Phys. Lett.*, **77**, pp. 450–452.
- [3] Lee, S., Demirci, M. U., and Nguyen, C. T.-C., 2001. "A 10-MHz micromechanical resonator pierce reference oscillator for communications". In Digest of Technical Papers, the 11 th Int. Conf. Solid-State Sens. & Actuators (Transducers'01), pp. 10–14.
- [4] Langdon, R., and Dowe, D., 1987. "Photoacoustic oscillator sensors". In SPIE Conf. Fiber Opt. Sens., pp. 86–93.
- [5] Stokes, N., Fatah, R. M., and Venkatesh, S., 1990. "Self-excitation in fiber-optic microresonator sensors". *Sens. Actuators A*, **21**, pp. 369–372.
- [6] Churenkov, A., 1993. "Photothermal excitation and self-excitation of silicon microresonators". *Sens. Actuators A*, **39**, pp. 141–148.
- [7] Hane, K., and Suzuki, K., 1996. "Self-excited vibration of a self-supporting thin film caused by laser irradiation". *Sens. Actuators A*, **51**, pp. 179–182.
- [8] Aubin, K. L., Zalalutdinov, M. K., Alan, T., Reichenbach, R. B., Rand, R. H., Zehnder, A. T., Parpia, J. M., and Craighead, H. G., 2004. "Limit cycle oscillations in CW laser-driven NEMS". *J. Microelectromech. Syst.*, **13**(6), pp. 1018–1026.
- [9] Zalalutdinov, M. K., Parpia, J. M., Aubin, K. L., Craighead, H. G., Alan, T., Zehnder, A. T., and Rand, R. H., 2003. "Hopf bifurcation in a disk-shaped NEMS". In Proceedings of the 2003 ASME Design Engineering Technical Conferences, 19th Biennial Conference on Mechanical Vibrations and Noise, pp. 1759–1769.
- [10] Sahai, T., Bhiladvala, R. B., and Zehnder, A. T., 2007. "Thermomechanical transitions in doubly-clamped micro-oscillators". *International Journal of Non-Linear Mechanics*, **42**(4), pp. 596–607.
- [11] Carr, D. W., Sekaric, L., and Craighead, H. G., 1998. "Measurement of nanomechanical resonant structures in single crystal silicon". *J. Vac. Sci. Technol. B*, **16**(6), pp. 3821–3824.
- [12] Pandey, M., Rand, R. H., and Zehnder, A. T., 2007. "Perturbation analysis of entrainment in a micromechanical limit cycle oscillator". *Commun. Nonlinear Sci. and Numer. Simul.*, **12**, pp. 1291–1301.
- [13] Pandey, M., Aubin, K. L., Zalalutdinov, M. K., Reichenbach, R. B., Zehnder, A. T., Rand, R. H., and Craighead, H. G., 2006. "Analysis of frequency locking in optically driven MEMS resonators". *J. Microelectromech. Syst.*, **15**(6), pp. 1546–1554.
- [14] Eisley, J. G., 1964. "Nonlinear vibration of beams and rectangular plates". *J. Appl. Math. Phys.*, **15**, pp. 167–175.
- [15] Eisley, J. G., 1964. "Large amplitude vibration of buckled beams and rectangular plates". *AIAA Journal*, **2**(12), pp. 2207–2209.
- [16] Timoshenko, S. P., 1955. *Vibration Problems in Engineering*, 3rd ed. D. Van Nostrand Company, INC.
- [17] Bouwstra, S., and Geijselaers, B., 1991. "On the resonance frequency of microbridges". In Digest of Technical Papers, Solid-State Sensors & Actuators (Transducers'91), pp. 538–542.
- [18] Ilic, B. R., Krylov, S., and Craighead, H. G., 2010. "Theoretical and experimental investigation of optically driven nanoelectromechanical oscillators". *J. Appl. Phys.*, **107**.
- [19] Blocher, D. B., Zehnder, A. T., Rand, R. H., and Mukerji, S. "Anchor deformations drive limit cycle oscillations in interferometrically transduced MEMS beams". *Submitted to Finite Elements in Analysis and Design (2011)*.
- [20] Sekaric, L., 2003. "Studies in NEMS : Nanoscale dynamics, energy dissipation, and structural materials". PhD thesis, Cornell University.
- [21] Doedel, E. J., Paffenroth, R. C., Champneys, A. R., Fairgrieve, T. F., Kuznetsov, Y. A., Oldeman, B. E., Sandstede, B., and Wang, X., 2002. *AUTO 2000: Continuation and Bifurcation Software for Ordinary Differential Equations (with HomCont)*.
- [22] Doedel, E. J., 2007. "Lecture notes on numerical analysis of nonlinear equations". In *Numerical Continuation Methods for Dynamical Systems: path following and boundary value problems*, B. Krauskopf, H. M. Osinga, and J. Gálán-Vioque, eds. Springer, pp. 1–49.
- [23] Zalalutdinov, M. K., Zehnder, A. T., Olkhovets, A., Turner, S. W., Sekaric, L., Ilic, B. R., Czaplewski, D. A., Parpia, J. M., and Craighead, H. G., 2001. "Autoparametric optical drive for micromechanical oscillators". *Appl. Phys. Lett.*, **79**(5), pp. 695–697.
- [24] Pandey, M., Rand, R. H., and Zehnder, A. T., 2008. "Frequency locking in a forced Mathieu-van der Pol-Duffing system". *Nonlinear Dyn.*, **54**, pp. 3–12.